# REPORT DOCUMENTATION PAGE

*Form Approved*
*OMB No. 0704-0188*



| 1. REPORT DATE *(DD-MM-YYYY)* | 2. REPORT TYPE | 3. DATES COVERED *(From - To)* |
|---|---|---|
| 03-01-2008 | Journal Article | |

**4. TITLE AND SUBTITLE**
Near-Inertial Currents in the DeSoto Canyon Region

**5a. CONTRACT NUMBER**

**5b. GRANT NUMBER**

**5c. PROGRAM ELEMENT NUMBER**
0601153N

**6. AUTHOR(S)**
Ewa Jarosz, Z.R. Hallock, William J. Teague

**5d. PROJECT NUMBER**

**5e. TASK NUMBER**

**5f. WORK UNIT NUMBER**
73-8554-A6-5

**7. PERFORMING ORGANIZATION NAME(S) AND ADDRESS(ES)**
Naval Research Laboratory
Oceanography Division
Stennis Space Center, MS 39529-5004

**8. PERFORMING ORGANIZATION REPORT NUMBER**
NRL/JA/7330-06-6287

**9. SPONSORING/MONITORING AGENCY NAME(S) AND ADDRESS(ES)**
Office of Naval Research
800 N. Quincy St.
Arlington, VA 22217-5660

**10. SPONSOR/MONITOR'S ACRONYM(S)**
ONR

**11. SPONSOR/MONITOR'S REPORT NUMBER(S)**

**12. DISTRIBUTION/AVAILABILITY STATEMENT**
Approved for public release, distribution is unlimited.

**13. SUPPLEMENTARY NOTES**

**14. ABSTRACT**
Near-inertial currents in the DeSoto Canyon region are described using current and wind observations taken between April 1997 and March 1998 for the "DeSoto Canyon Eddy Intrusion Study". Distinct energy peaks are present at near-inertial frequencies for the clockwise spectrum and there is little energy at the sam frequencies for the counterclockwise current spectrum. In this region, amplitudes of the near-inertial currents can be as high as 40 cm s-1. These currents are surface-intensified and display an increase in amplitude from the shelf break to offshore. Between November 1997 and March 1998, they were effectively generated by shifting winds accompanying passages of cold fronts. For this time period, near-inertial currents are reasonable well-simulated by a mixed-layer model forced by observed winds. During summer 1997, however, enhanced near-inertial motions often resulted from resonance between winds and existing currents.

**15. SUBJECT TERMS**
near-inertial currents, current-wind resonance, Gulf of Mexico, DeSoto Canyon

| 16. SECURITY CLASSIFICATION OF: | | | 17. LIMITATION OF ABSTRACT | 18. NUMBER OF PAGES | 19a. NAME OF RESPONSIBLE PERSON |
|---|---|---|---|---|---|
| a. REPORT | b. ABSTRACT | c. THIS PAGE | | | Ewa Jarosz |
| Unclassified | Unclassified | Unclassified | UL | 20 | 19b. TELEPHONE NUMBER *(Include area code)* 228-688-4292 |

Available online at www.sciencedirect.com
ScienceDirect
Continental Shelf Research 27 (2007) 2407–2426
CONTINENTAL SHELF RESEARCH
www.elsevier.com/locate/csr

# Near-inertial currents in the DeSoto Canyon region

E. Jarosz[a,*], Z.R. Hallock[b], W.J. Teague[a]

[a]*Naval Research Laboratory, Stennis Space Center, MS 39529, USA*
[b]*Planning Systems Incorporated, Slidell, LA 70458, USA*

Received 18 August 2006; received in revised form 1 June 2007; accepted 13 June 2007
Available online 10 July 2007

**Abstract**

Near-inertial currents in the DeSoto Canyon region are described using current and wind observations taken between April 1997 and March 1998 for the "DeSoto Canyon Eddy Intrusion Study". Distinct energy peaks are present at near-inertial frequencies for the clockwise spectrum and there is little energy at the same frequencies for the counterclockwise current spectrum. In this region, amplitudes of the near-inertial currents can be as high as $40\,cm\,s^{-1}$. These currents are surface-intensified and display an increase in amplitude from the shelf break to offshore. Between November 1997 and March 1998, they were effectively generated by shifting winds accompanying passages of cold fronts. For this time period, near-inertial currents are reasonably well-simulated by a mixed-layer model forced by observed winds. During summer 1997, however, enhanced near-inertial motions often resulted from resonance between winds and existing currents.
Published by Elsevier Ltd.

*Keywords:* Near-inertial currents; Current–wind resonance; Gulf of Mexico; DeSoto Canyon

## 1. Introduction

Near-inertial oscillations are common features observed in the open ocean and shelf seas. These oscillations are produced most effectively by an impulse of winds blowing for less than half of the local inertial period on the surface layer, and in ideal conditions, they may persist for several days after their generation. Inertial oscillations are seen as clockwise (CW) rotating, near-circular horizontal currents in the northern hemisphere, with frequencies slightly above the local inertial frequency (Pollard, 1970; Perkins, 1972; Kundu, 1976). Ultimately, these currents are gradually damped in shallow waters by bottom friction and/or out of phase winds (Davies, 1985; Orlic, 1987). Additionally, in stratified waters, the near-inertial energy is often reduced by leaking below the pycnocline due to the Ekman pumping (Weller, 1982) or by radiating from a generation region in a form of internal waves (Millot and Crepon, 1981).

Near-inertial currents are also ubiquitous in the shelf/slope region in the northern Gulf of Mexico. For example, Chen et al. (1996) and DiMarco et al. (2000) have described such phenomena on the Texas–Louisiana shelf. The DeSoto Canyon area in the northeastern Gulf extends over the same latitude range (28–30°N) as these earlier studies to the west. Near-nertial currents are usually generated by sudden changes in the surface wind stress associated with the local wind field (Pollard, 1970;

*Corresponding author.
*E-mail address:* ewa.jarosz@nrlssc.navy.mil (E. Jarosz).

0278-4343/$ - see front matter Published by Elsevier Ltd
doi:10.1016/j.csr.2007.06.014

Pollard and Millard, 1970; Perkins, 1972). In the northern Gulf of Mexico, however, these currents have approximately diurnal periods and they may be easily mistaken for currents generated by the dominant ($O_1$ and $K_1$) tidal constituents in the Gulf of Mexico (Henderschott, 1973). Additionally, near-inertial currents near 30°N may be associated with diurnal surface heating and cooling (DiMarco et al., 2000). Furthermore, near this latitude, the diurnal sea-breeze frequency is also very close to the local inertial frequency. Thus energetic near-inertial currents could be forced by the sea breeze (Lerczak et al., 2001; Simpson et al., 2002) or existing near-inertial currents may become significantly enhanced by resonance with this diurnal forcing. Finally, presence of near-inertial motions could be one of the most important factors in mixing across the pycnocline (Krausse, 1981; van Haren, 2000; Davies and Xing, 2004) in areas where tidal energy is low, such as in the northern Gulf of Mexico.

An extensive experiment, "DeSoto Canyon Eddy Intrusion Study" (Hamilton et al., 2000), was conducted in the DeSoto Canyon region over 2 years beginning in March 1997. This experiment included current, temperature, and conductivity moorings and hydrographic surveys. These observations were collected close to the critical latitude for diurnal motions. In this paper, we focus on the near-inertial signal recorded by the moored current meters as well as other observations pertinent to the near-inertial motion, including nearby wind velocities from meteorological stations. We attempt to answer the following questions using the DeSoto Canyon observations. Are near-inertial currents in the DeSoto Canyon region the result of high-frequency (near-inertial) wind forcing as found by Chen et al. (1996) for the northwestern Gulf of Mexico? Is there resonance between diurnal atmospheric forcing and near-inertial motion as found by DiMarco et al. (2000)? An outline of the paper is as follows. Analyzed observations are described in Section 2. Variability of near-inertial currents is shortly discussed in Section 3. Current spectra and variance for the near-inertial band are estimated and discussed in Section 4. Results from complex demodulation are presented in Section 5. In Section 6, based on results from a slab-like mixed-layer model, driving mechanisms of near-inertial currents are discussed. Resonance between diurnal atmospheric forcing and near-inertial currents is described in Section 7. Finally, a summary is given in Section 8.

## 2. Observations

The data used for this study were obtained from the DeSoto Canyon Experiment archives maintained by Science Applications International Corporation (www.saicocean.com). Logistics of the experiment, data return and descriptive analyses (some concerning near-inertial motions) can be found in Hamilton et al. (2000). Data used here are primarily from the 13 moored acoustic Doppler current profiler (ADCP) records and wind velocities from NDBC buoy 42040 and CMAN station DPIA1. Locations of the moorings and meteorological stations are shown in Fig. 1. Extensive hydrographic surveys were conducted during the deployment and recovery cruises; some of the CTD profiles adjacent to the moorings are also included in analyses.

Most of the time series data extend over the 2-year period from March 1997 to April 1999. The depth span covered by ADCP instruments varied among moorings but at most locations, the maximum depth was no more than 80 m, while the minimum depth was no less than 8 m. The ADCP bin size was 4 m except for the D9 mooring where 8.7-m vertical bins were used. The data in the archive were edited, and the ADCP data were low-pass filtered at 3 h (a Lanczos filter). The ADCP series at the A1 mooring are in four segments; the mooring was recovered and redeployed three times during the experiment. Moreover, the first of these started about 7 months later than the rest. The B1 record covers only the first year of the experiment. The wind velocity data from buoy 42040 has a gap in the second year, but is contiguous from March 1997 into October 1998, covering most of the experimental period, while the wind observations from DPIA1 cover the entire deployment period. Our analyses and discussion of findings will focus on the time period common to the A2–E1 moorings that is restricted by the length of observations from the B1 location. Thus almost all analyses will be performed for the current and wind data between April 1, 1997 and March 31, 1998.

Prior to the analyses, tidal currents were removed from the ADCP observations. Amplitudes and phases of the tidal constituents were computed using the tidal analysis program T_TIDE (Pawlowicz et al., 2002). The principal tidal constituents estimated and removed were $Q_1$, $O_1$, $P_1$, $K_1$, $N_2$, $M_2$, and $S_2$. Estimated amplitudes of the diurnal tidal currents in the upper (70–80 m) part of the

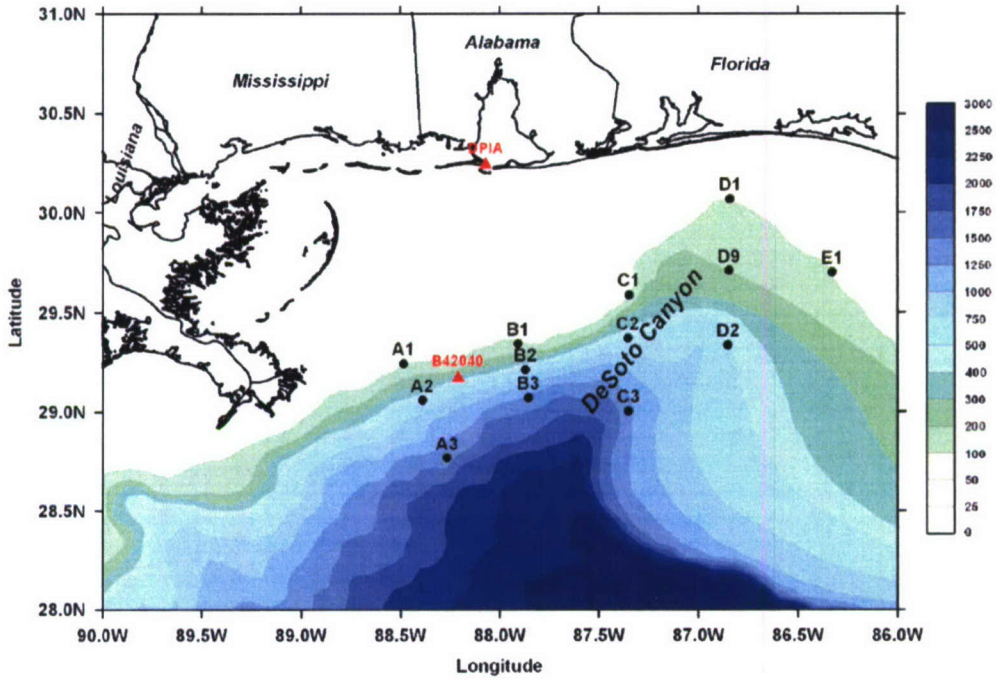


Fig. 1. Map of DeSoto Canyon region and moorings. Black dots are current, ADCP, and temperature/conductivity moorings. Red triangles are meteorological stations.

water column were usually below $5\,cm\,s^{-1}$, while those of the semidiurnal reached $2\,cm\,s^{-1}$. These small amplitudes are in good agreement with those estimated from a barotropic tidal model (He and Weisberg, 2002). The model estimates clearly show that both principle diurnal and semidiurnal currents are very small near the DeSoto Canyon when total depths are larger than 100 m (see Fig. 10 in He and Weisberg (2002)). Additionally, the variance of diurnal tides estimated by Molinari and Mayer (1982) from current observations collected just southwest of the canyon also implies that there is little energy in the tidal band.

## 3. Near-inertial current variability

In Figs. 2 and 3 we show samples of eastward and northward current velocity components from the 16 m bin of the A2 mooring, and of the wind velocity from NDBC buoy 42040. Both wind and current exhibit a broad spectrum of variability and show elevated energy near diurnal periods, especially evident in the current record. The quasi-diurnal fluctuations in the currents exhibit a phase lead for the northward component relative to the eastward component consistent with a CW rotation of the vector, which is a signature of inertial oscillations (Figs. 2(b) and 3(b)). This is generally not seen in the wind velocity observations.

Between October and May, near-inertial currents in the northern Gulf are mainly generated by shifting winds (Fig. 2(a)) associated with passages of atmospheric fronts (cold fronts) (Daddio et al., 1978; Chen et al., 1996). These fronts are very frequent and can appear in the Gulf every 3–10 days during this time of the year (DiMego et al., 1976). An example of near-inertial currents generated by frontal passages is well documented in the analyzed observations as shown in Fig. 2. Current oscillations excited by winds accompanying cold fronts can reach amplitudes as large as $40\,cm\,s^{-1}$ such as those between February 9 and March 11, 1997 shown in Fig. 2(b).

During the summer months (June–September), atmospheric frontal passages are very infrequent and near-inertial currents in the Gulf are usually induced by tropical storms, localized thunderstorms, and diurnal atmospheric forcing (sea breeze and daily heating and cooling). Those produced by a tropical storm are shown in Fig. 3. Near July 18, 1997, there is a sudden increase in inertial current energy (Fig. 3(b)), coincident with the rapid rise in wind velocity (Fig. 3(a)) caused by Hurricane Danny's passage. This burst decays exponentially

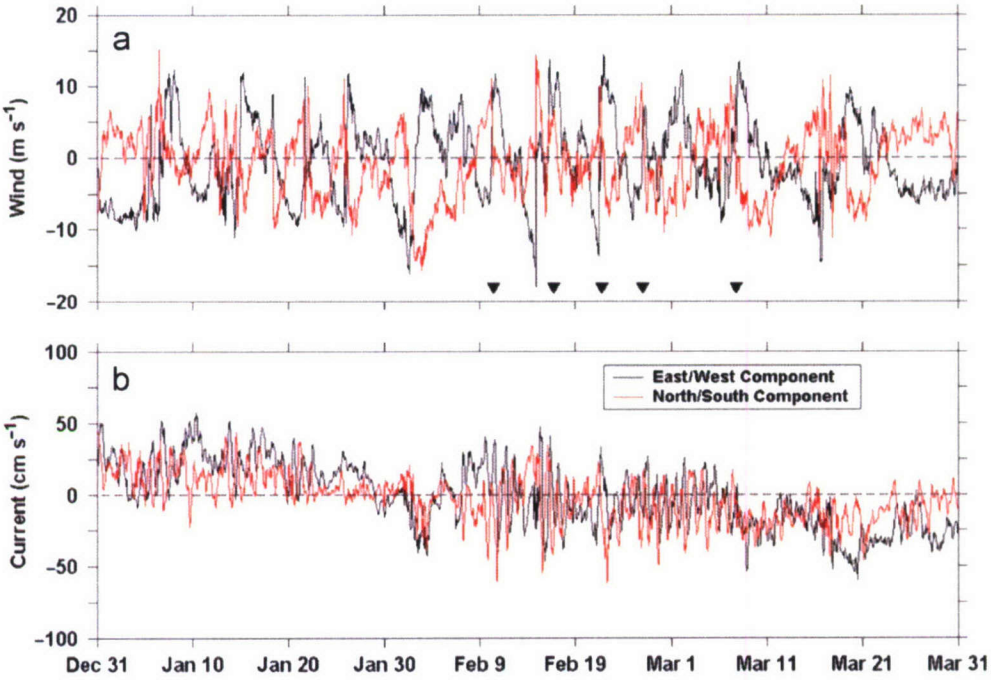


Fig. 2. Sample of east/west (black line) and north/south (red line) velocity components for (a) winds at buoy 42040 and (b) currents at the A2 mooring for nonsummer months; positive values are directed eastward and northward; passages of prominent cold fronts between February 9 and March 11, 1998 are marked by black triangles.

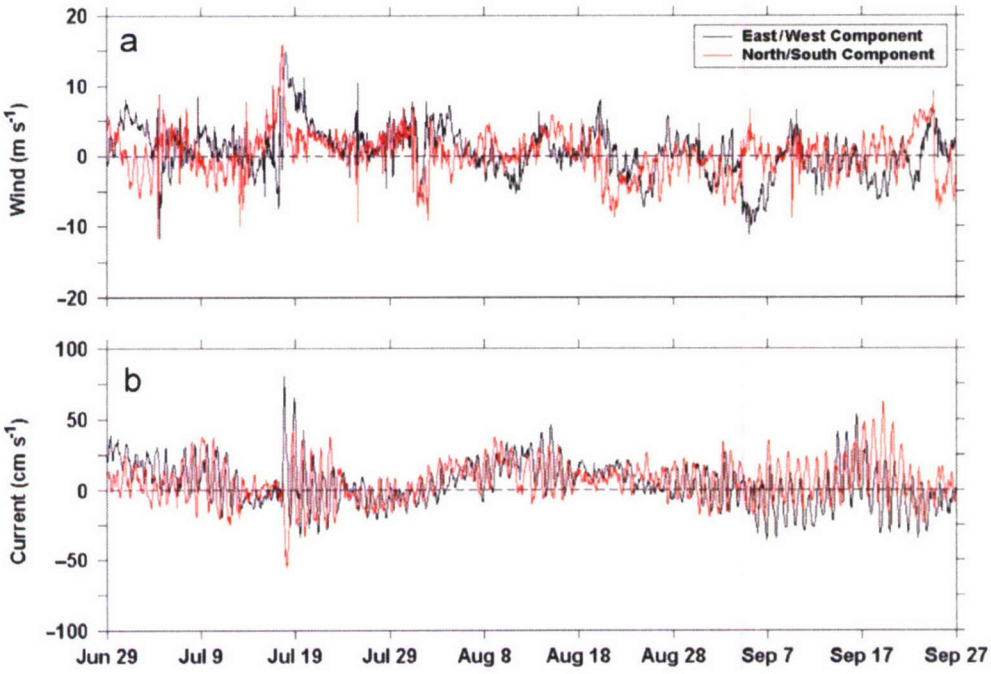


Fig. 3. Sample of east/west (black line) and north/south (red line) velocity components for (a) winds at buoy 42040 and (b) currents at the A2 mooring for summer months; positive values are directed eastward and northward.

over several days, as would be expected with impulse forcing (Price, 1983; Shay et al., 1998). Between July 9 and July 14, 1997 there is a smaller increase in inertial energy in the current associated with a smaller increase in the wind speed. On the other hand, a stronger wind event between June 29

and July 4, 1997 is accompanied by a decrease in current energy. As suggested by DiMarco et al. (2000) while near-inertial currents can be excited from relatively quiescent conditions by a strong broadband event such as hurricane Danny, in other cases they can be excited by a weaker, fluctuating wind, provided that the frequency and phase are favorable for reinforcement, or a resonance effect; an example of this is also evident in Fig. 3, particularly between September 12 and September 22, 1997 where inertial current continues to increase with steady and declining wind speed. The inertial current energy envelope near September 22 has a distinctly different character than that near July 19 (Fig. 3(b)). If the forcing is out of phase with an existing burst of near-inertial currents, the currents are suppressed (Crawford and Large, 1996). Phase relationships between winds and near-surface currents are examined in greater detail in Section 7.

The vertical structure of near-inertial currents generated by winds associated with the cold front and summer winds are displayed in Figs. 4(a) and (b), respectively. Detided current data were also band-passed (a sixth-order Butterworth 18–30 h band-pass filter) to isolate the near-inertial oscillations. These figures show only north/south velocity components registered by instruments in B1, B2, and B3 moorings. At the shelf break (B1 mooring), the near-inertial currents are characterized by a vertical structure in which currents reverse direction between 20 and 30 m, i.e., below the mixed layer. This reversal is related to the continuity condition imposed by the land boundary (Millot and Crepon, 1981; Federiuk and Allen, 1996), while the specific depth of the reversal is related to stratification which differs between summer and nonsummer months as discussed in the next sections. On the slope (B3), there is a well-defined upward phase propagation that is consistent with a downward energy flux as expected for motions with a source at the sea surface. Additionally, vertical distributions of phases (not shown) obtained from the empirical orthogonal function analyses (Denbo and Allen, 1984) clearly show this upward phase propagation and also allow us to estimate the vertical phase speed. This speed, for instance, at the B3 mooring during the summer months is, on average, $0.16\,\mathrm{cm\,s^{-1}}$ for the frequency of 1 cpd. Furthermore, phase differences between the upper depths (8–16 m) and those between 70 and 80 m are approximately 180° for nearly all locations. These differences seem to imply that vertical structure of near-inertial motions along the 100-m isobath in the DeSoto Canyon region are dominated by the lowest baroclinic modes.

## 4. Current spectra and variance at the near-inertial band

Rotary spectra of current records (Figs. 5(a) and (b)) show dominant CW energy at the near-inertial frequency. These spectra were estimated from the detided observations recorded at the 16-m depth for the A2, B2, and C2 moorings and the time interval between April 1, 1997 and March 31, 1998. CW current spectra are also shown for summer (June 1997–September 1997; Fig. 5(c)) and nonsummer (November 1997–March 1998; Fig. 5(d)) months for the same depth and moorings. For these time intervals, there are prominent peaks for the CW energy at the near-inertial frequency band while there is little energy for the counterclockwise (CCW) energy (not shown) at the same frequency band. Additionally, spectra shown in Figs. 5(c) and (d) imply that there is more CW energy in the DeSoto Canyon region in summer months than in nonsummer months. Finally, rotary spectra for wind data recorded at DPIA and buoy 42040 for summer and nonsummer months (the same time periods as for current observations) were also estimated (Fig. 6). These spectra display distinct peaks in the diurnal band for the CW energy. They also show some decrease of the CW energy in the diurnal band for the wind velocity from summer (Fig. 6(a)) to nonsummer months (Fig. 6(b)). As found by DiMarco et al. (2000) for the northwestern Gulf, this difference for the CW wind energy may be associated with diurnal heating/cooling and sea breeze effects, more prevalent in the summer.

The actual peak in the CW spectrum for currents depends on location and falls between 0.93 cpd (cycle per day) and 1.05 cpd, while the local inertial frequency varies between 0.96 and 1 cpd. The frequency resolution, however, is approximately 0.1 cpd so the difference is not significant. It is generally expected that inertial motions occur at frequencies slightly above the local inertial frequency ($f$) if they are to exist as free waves (Perkins, 1972; Kundu, 1976) but Doppler and horizontal shear effects may depress the effective value of $f$ (Kunze, 1985). The CW spectrum peak for the wind is at 1.05 cpd, consistent with the proposition that diurnal atmospheric effects are present.

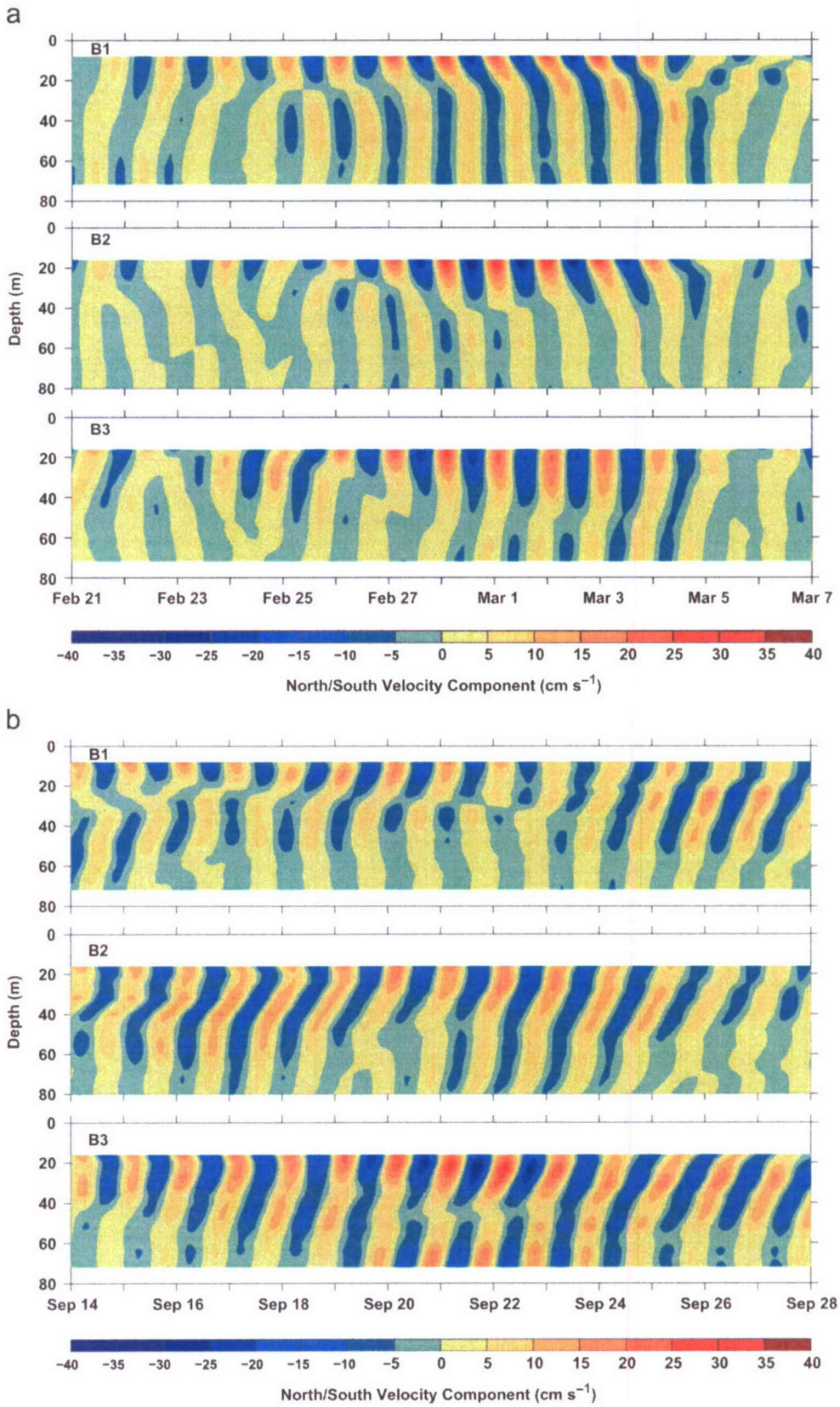


Fig. 4. Vertical structure of near-inertial currents excited by (a) a cold front passage and (b) summer winds; the north/south current velocity components have been detided and band-passed (18–30 h); positive values are directed northward.

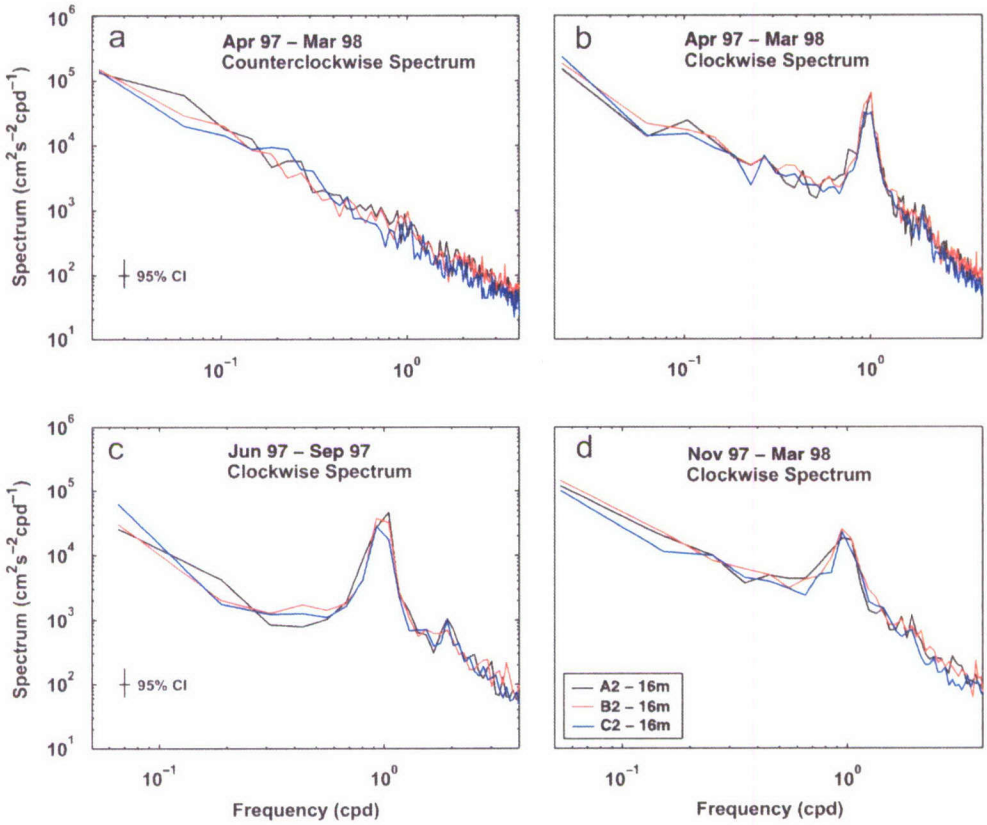


Fig. 5. Rotary spectra of 16 m current velocities for the A2, B2, and C2 moorings: (a) counterclockwise and (b) clockwise spectra estimated for the time period between April1 1997 and March 31, 1998, (c) clockwise spectra for summer months (June 1, 1997–September 31, 1997), and (d) clockwise spectra for nonsummer months (November 1, 1997–March 31, 1997).

The estimated CW spectra were used to estimate current variance in the near-inertial band. Fig. 7 shows the averaged variance for currents measured at 20 m between April 1, 1997 and March 31, 1998. The variance distribution clearly indicates that near-inertial energy increases from the shelf break to offshore, and that near-inertial currents are the most energetic at the A3, B3, and C3 locations. This distribution is very different to that found in the northwestern Gulf where near-inertial currents have a maximum at the shelf break and diminish gradually toward the coast and rapidly offshore (Chen et al., 1996). The lowest near-inertial energy at the shelf break in the DeSoto Canyon region is probably related to the fact that the shelf break in this area is near the 30°N latitude (see Figs. 1 and 7). North of this latitude freely propagating internal diurnal waves are not supported but instead are refracted back towards the equator. Thus less energy is allocated in the near-inertial band as locations of the shelf break moorings approach this latitude (Fig. 7).

When variance is estimated from the CW spectrum separately for the summer and nonsummer time intervals an offshore increase of near-inertial energy is also apparent, as shown in Fig. 8 for the C1, C2, and C3 moorings when compared at the same depth. The largest differences in near-inertial variance are generally found in the upper 30–40 m, except at A2 and A3 where the estimated variance is comparable. The differences are more prominent for the summer time period. Additionally, vertical variance distributions at all C moorings indicate that near-inertial currents are surface intensified. This surface intensification is also present at other locations as expected for motions excited by surface wind forcing.

## 5. Complex demodulation of wind and current velocity

We first examine the near-inertial current content of the bins of all available ADCPs as well as the rotary component makeup of the wind velocity

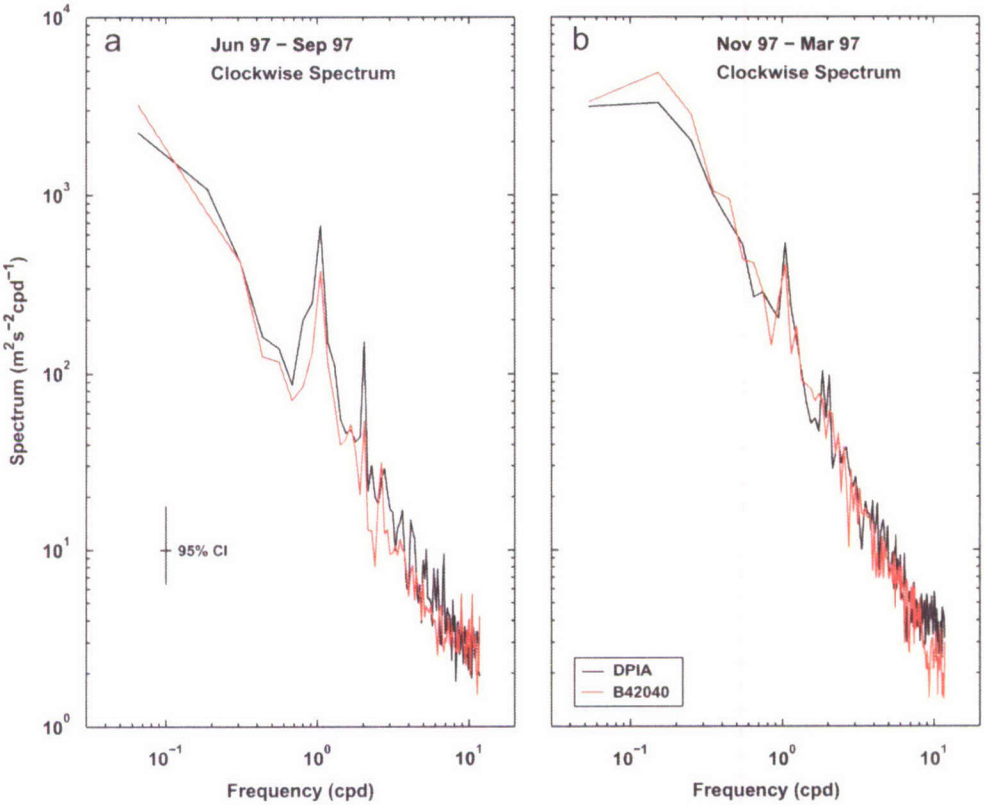


Fig. 6. Clockwise spectra of wind velocities measured at the CMAN station DPIA and buoy 42042 for (a) summer months (June 1, 1997–September 31, 1997), and (b) nonsummer months (November 1, 1997–March 31, 1997).

record at the NDBC buoy 42040. Complex demodulation (Perkins, 1976) applied to velocity data, which have been band-pass filtered between the periods of 3 and 40 h (a sixth-order Butterworth filter), yields CW and CCW components for a specified frequency. The filter removes long-period trends and high-frequency noise, resulting in a cleaner presentation. The CW and CCW components of the near-inertial currents were estimated for a frequency of 1 cpd.

In the northern hemisphere, inertial oscillations are characterized by CW rotation so at 30°N we would expect the CW current component to be dominant in the diurnal band. Wind generation of inertial oscillations requires that the forcing have a CW component at or near the local inertial frequency. A CCW can also be present as in the case of a rectilinear wind where the CW and CCW amplitudes are equal. It is essential that the wind and current be positively correlated in the vector sense. Simpson et al. (2002) calculated a resonant response dependence on the latitude for diurnal CW and CCW wind stress components acting on a shallow mixed layer, and found that near 30°N, the CW component is dominant.

CW and CCW amplitudes of the wind and CW amplitudes of the near-inertial currents are shown in Figs. 9–11. While there is generally more CW than CCW wind energy (Fig. 9), CCW amplitudes are significant and occasionally exceed CW amplitudes. For the currents (Figs. 10 and 11), the CW component dominates. CW amplitudes are mainly between 10 and 30 cm s$^{-1}$ but they often reach values of 40 cm s$^{-1}$ while the largest CCW amplitudes (not shown) are generally below 7 cm s$^{-1}$ between April 1, 1997 and March 31, 1998. While wind speeds are generally higher from late fall to early spring in the northern Gulf of Mexico (Gutiérrez de Velasco and Winant, 1996), the near-inertial amplitudes tend to be higher in the summer. Distributions of the CW amplitudes confirm conclusions derived from the variance distributions, i.e., (1) near-inertial motions are more energetic in summer months, and (2) the strength of near-inertial currents increases offshore from the shelf break in the DeSoto Canyon region.

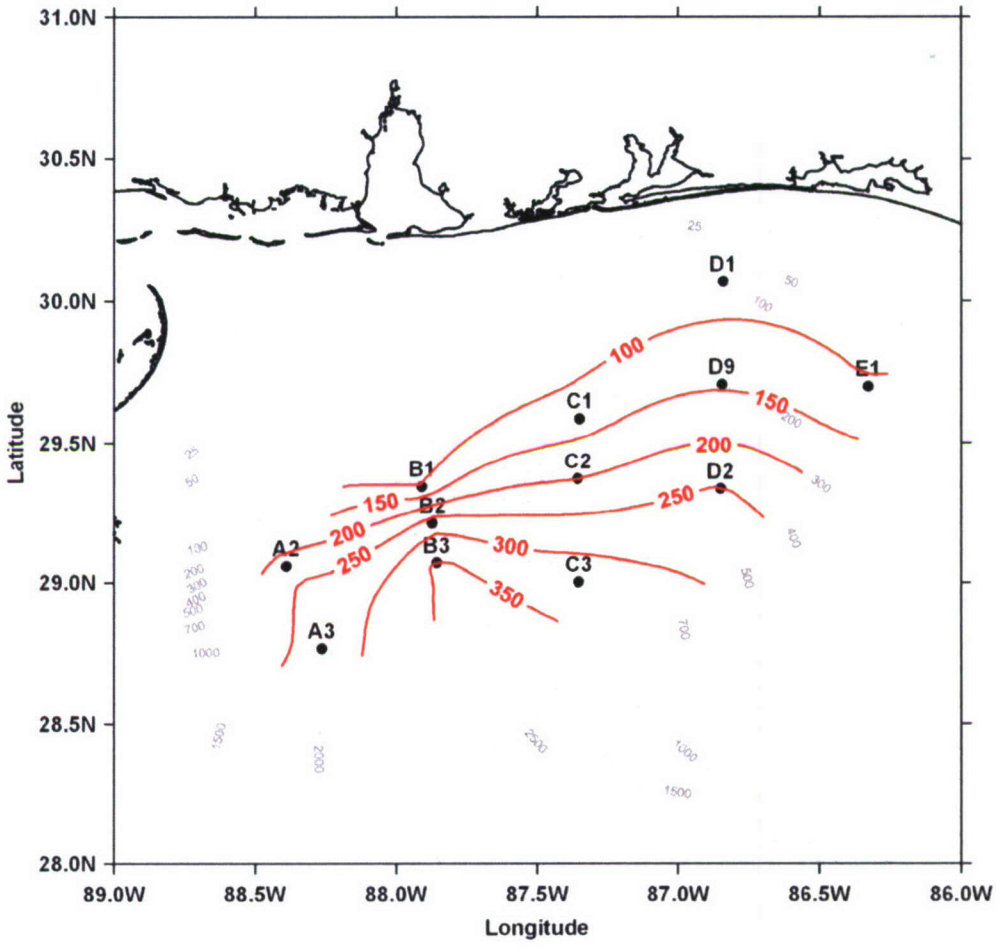


Fig. 7. Clockwise variance ($cm^2 s^{-2}$) of near-inertial currents at 20 m estimated for the time period between April 1, 1997 and March 31, 1998.

Stratification and mixed-layer depths in the northern Gulf of Mexico differ from one season to another and can be highly influenced by fresh water discharges from local rivers, primarily from the Mississippi River whose annual discharge is about $19{,}000\,m^3 s^{-1}$ (Wiseman et al., 1997). The greatest impact of riverine waters on stratification and on mixed-layer depths is historically observed in summer when the largest volume of low salinity waters is present (Hamilton et al., 2000; Jochens et al., 2002; Morey et al., 2003). For a given forcing amplitude, an induced near-inertial amplitude will be greater for a shallow mixed layer that is effectively decoupled from the deeper water by a strong pycnocline (D'Asaro, 1985; Shearman, 2005). Such conditions are met during the summer in the northern Gulf. Typical profiles of density ($\sigma_\theta$) near the A2, B2, C2, and D2 mooring sites (Fig. 12) show changing conditions with season. A pycnocline was established early in 1997 and deepened in the summer (Figs. 12(a) and (b)). The following fall (Fig. 12(c)), most of the pycnocline was mixed away before the CTD survey. Spring (Fig. 12(d)) had no shallow pycnocline. Thus the difference in the amount of near-inertial energy near the DeSoto Canyon is certainly related to differences in stratification observed in the summer and nonsummer months, i.e., a shallower mixed layer present between June and September 1997 was more inducive to wind forcing generating the near-inertial motion. However, the offshore increase of this energy, i.e., the largest amplitudes observed in the summer and nonsummer months at A3, B3, and C3 could result from energy trapping due to the presence of a negative relative vorticity field generated by mesoscale circulation (Hamilton et al., 2000). The negative vorticity reduces the effective frequency of near-inertial motion so that the motion becomes

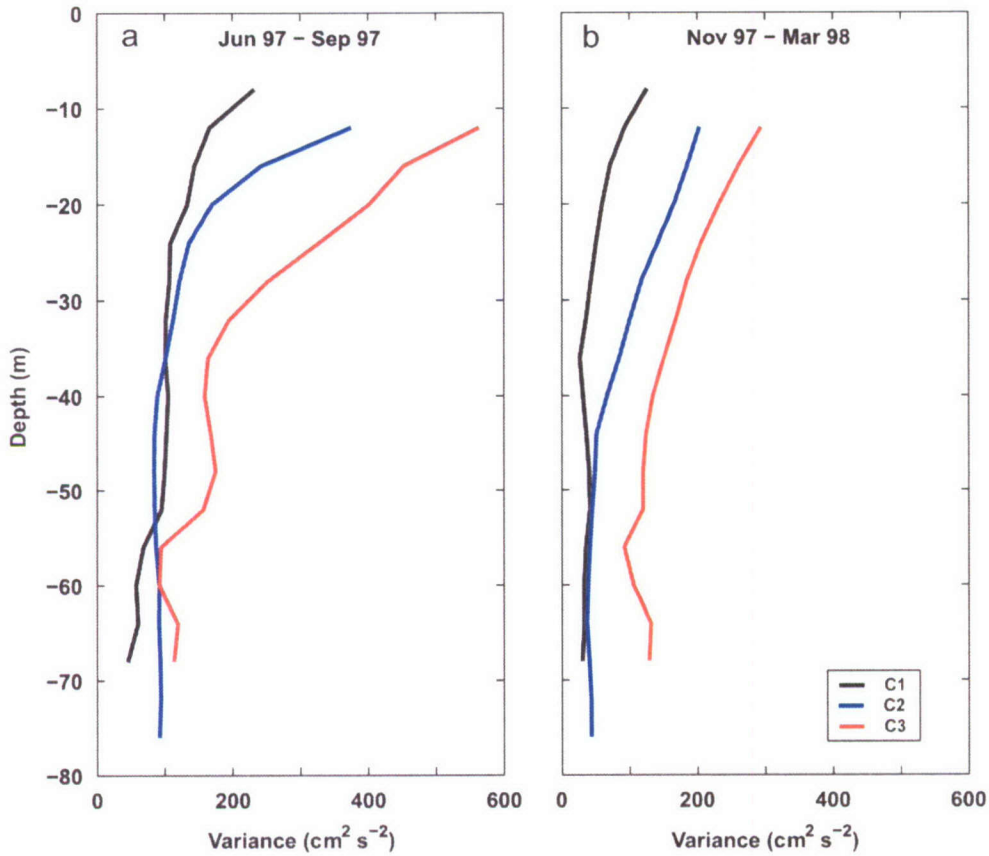


Fig. 8. Vertical distributions of clockwise variance for the near-inertial currents recorded at C1, C2, and C3 moorings during (a) summer (June 1, 1997–September 31, 1997) and (b) nonsummer (November 1, 1997–March 31, 1997) months.

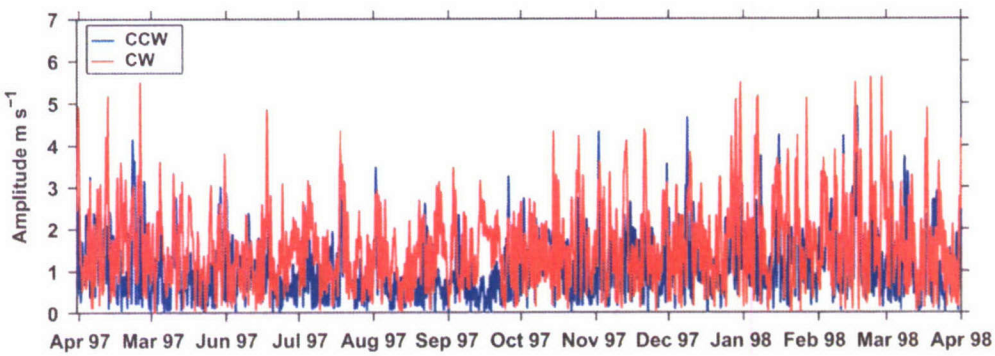


Fig. 9. Clockwise (CW) and counterclockwise (CCW) amplitudes of winds recorded at buoy 42040 and obtained from complex demodulation for a frequency of 1 cpd.

subinertial, trapped, and amplified in regions of negative relative vorticity (Kunze, 1985; D'Asaro, 1995). Figs. 13(a) and (b) show respectively the near-inertial amplitudes at 20 m estimated for the C1, C2, and C3 moorings and vorticity estimated at C3 following a procedure described by Chereskin et al. (2000). These two figures show that when vorticity is negative the amplitudes at C3 can be more than $10\,\mathrm{cm\,s^{-1}}$ larger than those at C1 and C2. It should be also noted that the mooring setup is not particularly well suited for computations of vorticity. Thus while uncertainty in the absolute value of the vorticity displayed in Fig. 13(b) may be high, its temporal change is meaningful near the C3 mooring.

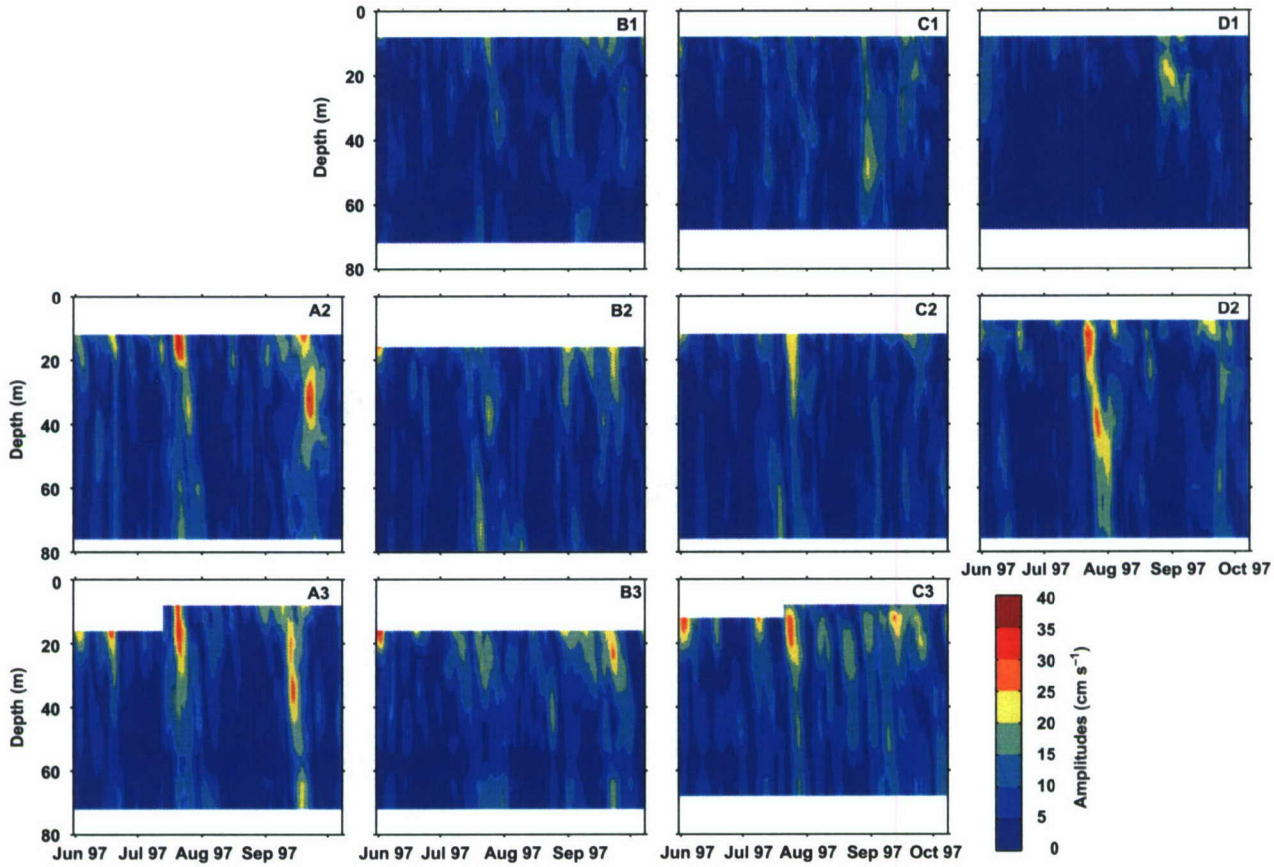


Fig. 10. Clockwise amplitudes of near-inertial currents recorded in the DeSoto Canyon region during summer of 1997, obtained from complex demodulation for a frequency of 1 cpd.

In stratified waters, enhanced amplitudes of near-inertial currents at A3, B3, and C3 coulds also result from a presence of offshore-propagating near-inertial internal waves. Numerous modeling efforts show that these waves are generated either at the coast as a consequence of upwelling/downwelling effects or at frontal regions separating well-mixed coastal and stratified ocean waters due to Ekman pumping (see, for example, Tintoré et al., 1995; Davies and Xing, 2004, 2005). Additionally, the observed spatial amplitude variation for the same near-inertial current episode could result from differences in existing stratification (for instance, due to bottom and/or surface fronts) and bathymetry. Finally, the distribution of the CW amplitudes below 40 m at the shallowest moorings could be partly related to the width of the shelf. The amplitudes are larger where the shelf is broader (for example, compare amplitudes below 40 m at B1 and D1 moorings). Results from modeling efforts by Xing and Davies (2003) suggest that this dependence, on short-time scales, relates to the surface elevation gradient which drives near-inertial currents below the pycnocline and whose magnitude depends on the water depth, i.e., it decreases as the water depth increases because of the continuity constraint.

## 6. Simulation of near-inertial currents by wind stress

Occurrences of near-inertial currents in the northern Gulf of Mexico are closely related to temporal variations of the low-frequency wind field. These variations, i.e., rapid changes in wind amplitude and direction are usually observed during cold front passages. In the northwestern Gulf, Chen et al. (1996) concluded that near-inertial currents were most effectively generated by near-diurnal (high-frequency) variations of the wind stress accompanying a passage of a cold front.

To understand importance of low- and high-frequency variations of the wind to amplitudes of near-inertial motion in the northeastern Gulf of Mexico, we employed a model developed by Pollard

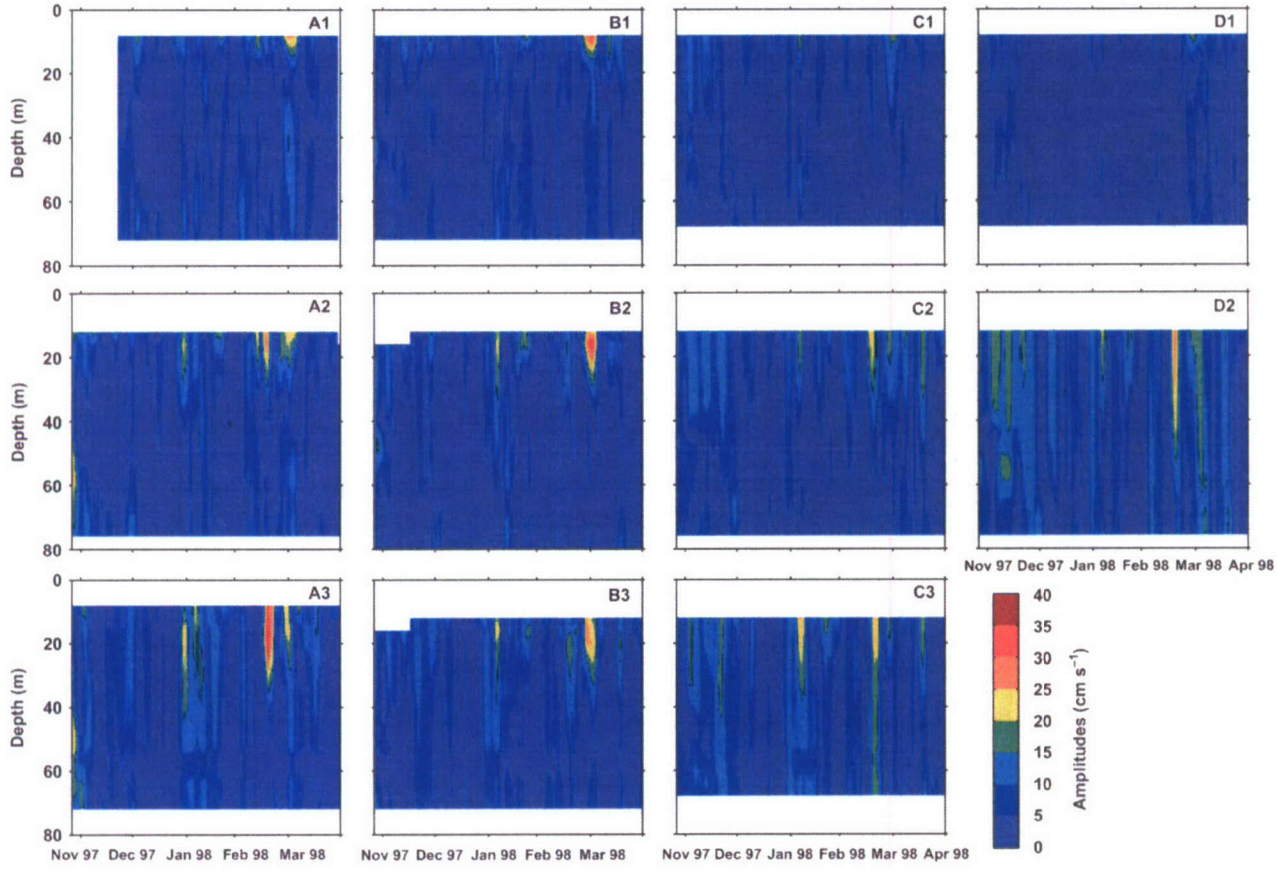


Fig. 11. Clockwise amplitudes of near-inertial currents recorded in the DeSoto Canyon region during nonsummer months, obtained from the complex demodulation for a frequency of 1 cpd.

and Millard (1970) whose equation in a complex form is given by (Chen et al., 1996)

$$\frac{dU}{dt} + f'U = \tau_s \tag{1}$$

where $U = hu + ihv$, $\tau_s = (\tau_{sx} + i\tau_{sy})/\rho_0$, $f' = C_0 + if$, $u$ and $v$ are the depth-averaged current velocities in the east/west and north/south directions, $\tau_{sx}$ and $\tau_{sy}$ are the east/west and north/south wind stress components, $h$ is the thickness of the mixed layer, $C_0$ is the drag coefficient of the internal wave radiation propagating away from the base of the mixed layer, $f$ is the local inertial frequency, and $\rho_0$ is the density in the mixed layer. The transport $U$ consists of the Ekman transport ($U_E$) and inertial motion ($U_I$). The inertial motion then can be estimated as follows:

$$U_I(t) = -\int_0^t \frac{1}{f'}\frac{d\tau_s}{dt} e^{-f'(t-t')}\, dt', \tag{2}$$

where $U_I$ is initially assumed to be zero.

Winds recorded at NDBC buoy 42040 were used to estimate wind stress components following an approach proposed by Large and Pond (1981). We chose to use only winds for the nonsummer months (November 1, 1997–March 31, 1998), i.e., for the time period when passages of cold fronts are historically very frequent in the northern Gulf of Mexico. The model was forced by the 40-hour, low-passed and hourly (both high- and low-passed) wind stresses to evaluate quantitatively contributions of low- and high-frequency wind variability to near-inertial motions. Complex demodulation was employed to extract CW amplitudes of the simulated near-inertial currents. These amplitudes were then compared with those found at A2. We chose near-inertial currents recorded at the A2 mooring for this comparison because of the proximity of the A2 mooring to the meteorological buoy. This choice should minimize possible phase differences between the forcing and the resulting near-inertial currents.

Examples of predicted and observed CW amplitudes are shown in Fig. 14. The best agreement is

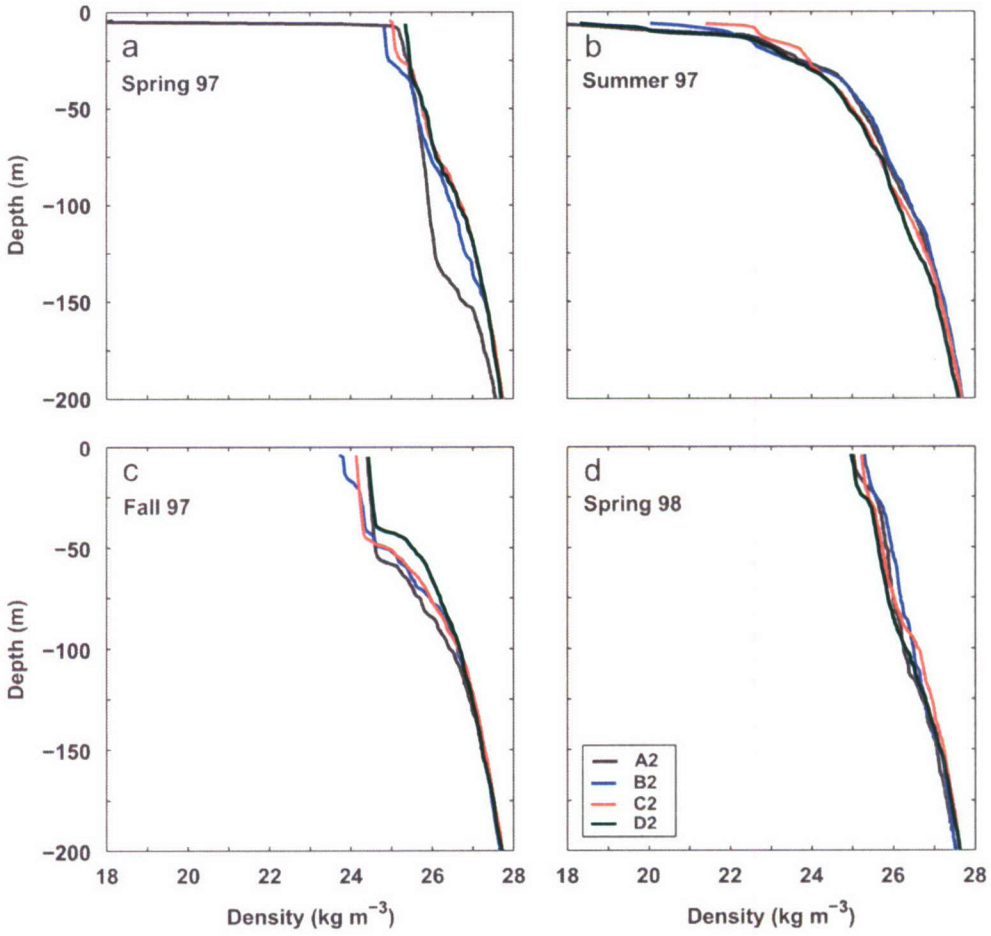


Fig. 12. Profiles of density ($\sigma_t$) from CTD casts near A2, B2, C2, and D2 for (a) spring 1997, (b) summer 1997, (c) fall 1997, and (d) spring 1998.

obtained for $C_o = 4.63 \times 10^{-6}\,s^{-1}$ ($\sim 2.5\,days^{-1}$). Comparison of these amplitudes shows that the amplitudes simulated by the hourly wind stress are in reasonable agreement with those recorded at A2, especially when the near-inertial motion is very energetic such as that generated between February 9 and March 9, 1998. Discrepancies between observed and modeled amplitudes could arise from not including processes such as mixing, leaking of near-inertial energy below the mixed layer, propagation of internal waves into the model region, and trapping of the near-inertial energy by mesoscale circulation.

As discussed, for example, by Xing and Davies (2003), sub-inertial winds are much less effective at generating near-inertial motions in the ocean. Amplitudes of near-inertial currents simulated by a low-passed wind stress (Fig. 14) support the above conclusion. The amplitudes generated by the low-frequency wind stress are very small when compared with those observed at the A2 location. Even though large near-inertial currents usually occur when the wind rapidly changes its direction during frontal passages, the amplitudes of the near-inertial motion excited by low-frequency winds are rather negligible. Thus energetic near-inertial currents in the DeSoto Canyon region during the time period between November 1, 1997 and March 31, 1998 were produced by the high-frequency (near-inertial) variation of wind field associated with passages of the cold fronts. Our conclusions regarding high- and low-frequency winds as forcing mechanisms of the near-inertial motion are identical to those presented by Chen et al. (1996) for the northwestern Gulf of Mexico.

## 7. Current–wind resonance

In the following section we focus on a more quiescent (nonstorm) time period. This time period

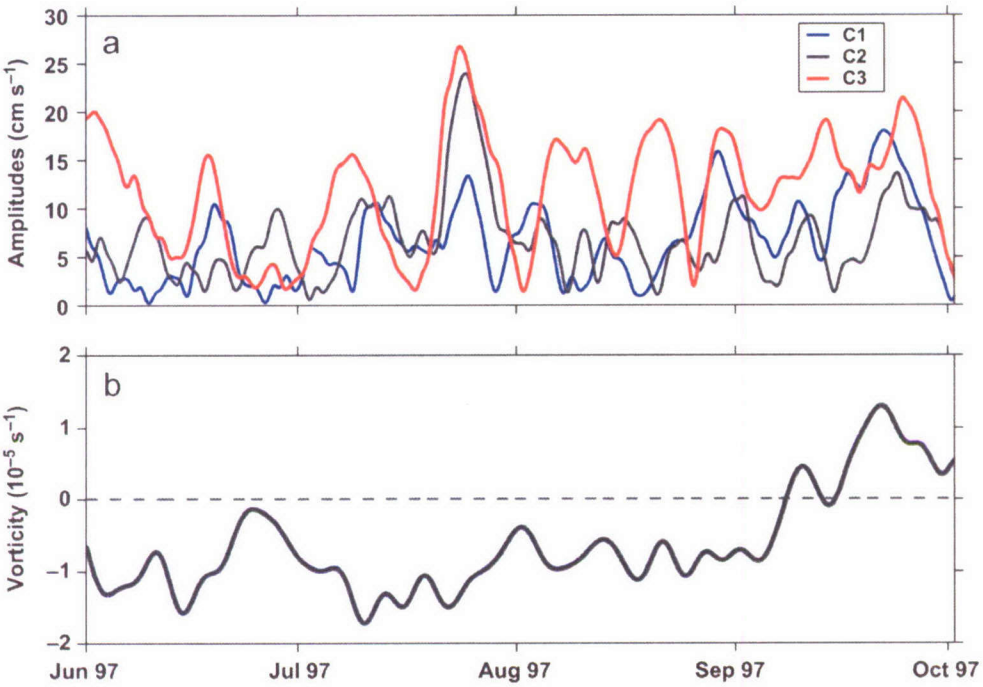


Fig. 13. (a) Clockwise amplitudes of 20 m near-inertial currents observed at the C1, C2, and C3 moorings, and (b) vorticity at 20 m estimated for the C3 mooring.

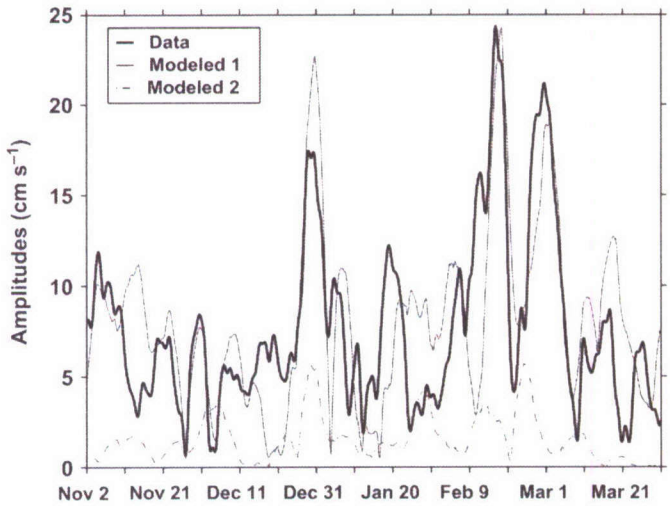


Fig. 14. CW amplitudes of observed (solid thick line) near-inertial currents at 16 m at the A2 mooring, simulated near-inertial currents using the hourly wind stress (solid thin line: Modeled 1), and simulated currents using 40-h low-frequency wind forcing (dot–dashed line: Modeled 2).

covers summer 1997, when diurnal resonant wind forcing of near-inertial motions such as found by DiMarco et al. (2000) is more likely to be observed. Two criteria must be met for such forcing to be effective: (1) the frequency of the forcing must be close to the inertial frequency; and (2) the forcing must be in phase with the near-inertial motions, once they have been established. If these criteria are met, the CW amplitude should grow in response to a steady-amplitude forcing function.

As before, we apply a diurnal band-pass filter (18–30 h) to the wind and current data. Subsequent analysis and discussion deal with these band-passed data. The filtered current observations from the

shallowest bins from the 11 sites (A1 and D9 are excluded) are then subjected to a time-domain complex principal component (PC) analysis (Preisendorfer, 1988). We do this because there are differences among the records, possibly caused by local effects such as stratification changes or interaction with subinertial flows. Since the wind field as measured at the buoy location is likely to be coherent over the moorings selected, it is reasonable to expect the directly forced portions of near-inertial energy at the different sites to be coherent. PC analysis identifies such coherence. The analysis is based on the expansion:

$$W(x_i, t_k) = \sum_{n=1}^{N} Z_n(t_k) E_n(x_i). \quad (3)$$

The horizontal positions of the moorings are indicated by $x$ and time by $t$. The eigenfuctions ($E_n$) of the covariance matrix of $W$ ($W = U + iV$, where $U$ and $V$ are east/west and north/south current velocity components, respectively), are orthonormal. The $Z_n$ (amplitudes or principal components) are orthogonal, and each carries the variance of its corresponding mode, $n$, equal to the eigenvalue (EV) associated with the mode. PC analysis is useful when the first one or two modes are clearly dominant, and the eigenfuctions exhibit meaningful structure. In this case, $E_n$ and $Z_n$ are complex and have both magnitude and phase. Essential statistics from the analysis are listed in Tables 1 and 2.

The EVs (Table 1) show robust first-mode dominance: its variance is more than twice the total of the remaining variance. Furthermore, the magnitude of the mode-1 eigenfunction (or EOF1) (Table 2) is nearly constant over 9 of the 11 moorings, with magnitudes for D1 and E1 significantly lower. Phase differences ($\mathrm{TAN}^{-1}E_1$ is relative to B3 which has the largest amplitude) are relatively small (except for D1 and E1), with a maximum of 2.72 h (assuming a diurnal period). Since the sampling interval is 1 h and data have been band-pass filtered between 18 and 30 h, these differences are probably not meaningful. The 4th column in Table 2 lists percent variance explained (PVE) for the corresponding mooring record. Low PVE generally corresponds to low eigenfuction magnitudes (D1, E1 and, to a lesser extent, C1). The last column in Table 2 lists the velocity variance for each record; their sum equals the sum of the EVs (column 2 of Table 1).

Table 1
Modal statistics

| Mode | EV ($cm^2 s^{-2}$) | EV (%) |
|---|---|---|
| 1 | 1142 | 57.1 |
| 2 | 255 | 12.8 |
| 3 | 142 | 7.1 |
| 4 | 118 | 5.9 |
| 5 | 83 | 4.1 |
| 6 | 75 | 3.7 |
| 7 | 53 | 2.6 |
| 8 | 50 | 2.5 |
| 9 | 39 | 2.0 |
| 10 | 24 | 1.2 |
| 11 | 17 | 0.9 |

EV is the eigenvalue.

Table 2
Mode-1 eigenfunctions

| Site | $\lvert E_1\rvert$ | $\mathrm{Tan}^{-1} E_1$ (h) | PVE (%) | Var ($cm^2 s^{-2}$) |
|---|---|---|---|---|
| A2 | 0.30 | 1.27 | 50 | 203 |
| A3 | 0.31 | 1.07 | 59 | 191 |
| B1 | 0.27 | 0.54 | 62 | 134 |
| B2 | 0.36 | 0.08 | 79 | 189 |
| B3 | 0.43 | 0.00 | 79 | 269 |
| C1 | 0.22 | 2.72 | 43 | 129 |
| C2 | 0.33 | 1.70 | 68 | 183 |
| C3 | 0.37 | 1.08 | 63 | 249 |
| D1 | 0.09 | 8.21 | 9 | 100 |
| D2 | 0.32 | 2.12 | 55 | 210 |
| E1 | 0.13 | 6.46 | 14 | 140 |

$|E_1|$ is the first mode magnitude, $\mathrm{Tan}^{-1} E_1$ is the first mode phase, PVE is the percent variance explained, *Var* is the velocity variance

The amplitude ($Z_1$) of the first mode is given by

$$Z_1(t_k) = \sum_{i=1}^{N} E_1^*(x_i) W(x_i, t_k), \quad (4)$$

where (*) indicates the complex conjugate. $Z_1$ has units of velocity; the real and imaginary parts of $Z_1$ are hence $U_1$ and $V_1$. We use $Z_1$ as representing mode-1 current velocity in subsequent analysis, but Eq. (3) should be used to derive modal velocities comparable to observed velocities, $W$.

The mode-1 velocity components, $U_1$ and $V_1$, are plotted on an expanded scale for the period of the sustained near-inertial current burst near September 6, 1997 in Fig. 15(a). Inertial-band-pass-filtered wind velocities, $U_w$ (the east/west component) and $V_w$ (the north/south component) (Fig. 15(b)) are also shown for the same time

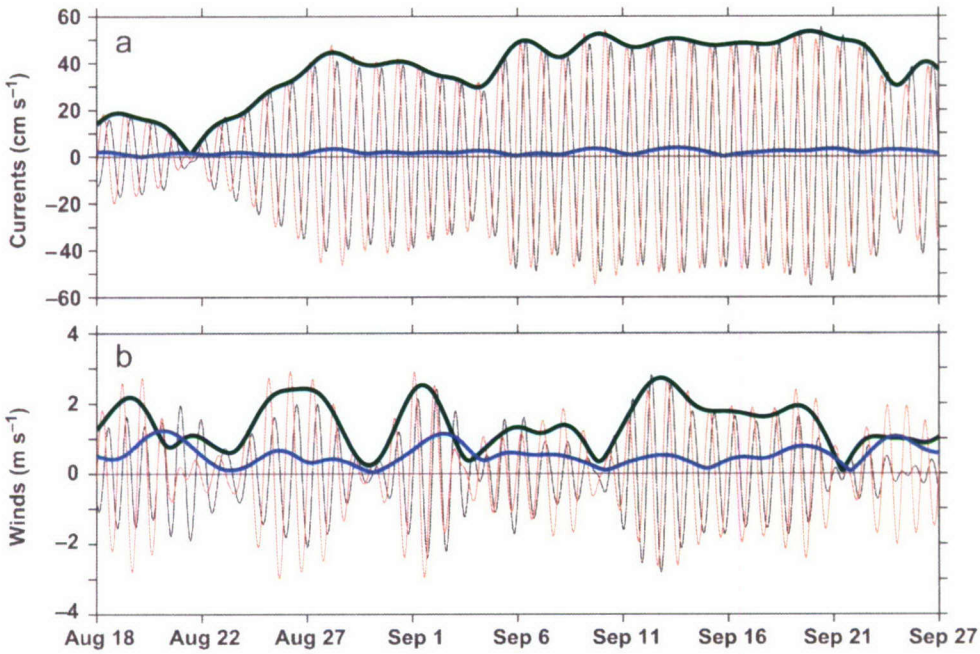


Fig. 15. (a) $U_1$ (black line) and $V_1$ (red line) components derived from principal component analysis of band-pass filtered upper-bin ADCP velocities from moorings A2–E1 for the first EOF mode (see text), and CW (green line) and CCW (blue line) amplitudes of the first EOF mode. (b) Band-pass filtered wind velocity components $U_w$ (black line) and $V_w$ (red line), and CW(green line) and CCW (blue line) wind amplitudes obtained from complex demodulation for a frequency of 1 cpd.

period. Superimposed are the CW and CCW magnitudes calculated from complex demodulation for $Z_1$ and $W_w$ ($W_w = U_w + iV_w$). Dominance of the CW component is evident for the currents and winds; however, significant CCW amplitudes are also present for the winds. There is no obvious correlation between energy levels for the currents and winds shown in Fig. 15. However, there are times when the wind velocity fluctuations are positively correlated with the currents, hence reinforcing the near-inertial currents. There are also times when they are negatively correlated so that the wind forcing reduces near-inertial current fluctuations. The effectiveness of the forcing of near-inertial currents depends on the relative phase between the wind velocity components ($U_w$, $V_w$). The wind forcing is optimal if the wind vector rotates CW (as do the near-inertial current vectors) and the wind is in phase overall with the existing near-inertial currents. If there is no near-inertial energy initially, the latter requirement is moot. The optimal forcing is not necessary to generate near-inertial currents. It is necessary only to have a positive vector correlation between the vectors. This occurs when there is a CW component in the forcing; a CCW component may also be present, as in the case of a rectilinear wind (equal CW and CCW amplitudes). The phase relationships are illustrated with an expanded plot (Fig. 16) for the time period between August 23 and September 7, 1997. Figs. 16(a) and (b) show eastward and northward velocity components of the band-passed current and wind. Around August 28 the wind and current are nearly in phase, and as long as wind energy is present, the current fluctuations grow. Around noon on August 30, the wind amplitude approaches zero and the current amplitude levels off and decreases slightly. The wind again increases in amplitude starting around September 1 but is no longer in phase with the current. By September 5 the current amplitude has decreased to a local minimum. These relationships can be quantified by examining the covariance between the current and wind. We define a complex covariance (Kundu, 1976)

$$Covc = \overline{Z_1^* W_w}, \tag{5}$$

where (*) indicates complex conjugate and the overbar indicates a low-pass filter. The real part of Eq. (5) is the vector covariance. For direct comparison with the wind speed, *Covc* is divided by the smoothed current speed, $\overline{|Z_1|}$

$$Cov' \equiv \frac{\mathrm{Re}\{Covc\}}{\overline{|Z_1|}} = \frac{\overline{U_1 U_w + V_1 V_w}}{\overline{|Z_1|}}. \tag{6}$$

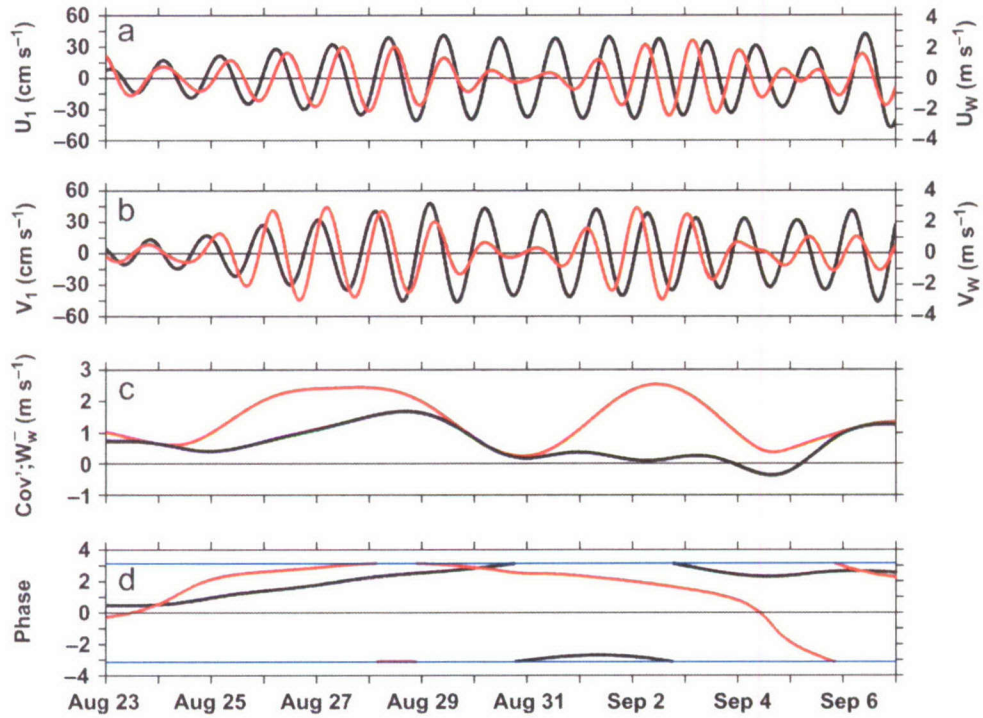


Fig. 16. (a) $U_1$ (black line) and $U_w$ (red), (b) $V_1$ (black line) and $V_w$ (red line), for a 15-day period. (c) $Cov'$ (black line) and $|W_w^-|$ (red line). (d) CW current phase ($\phi$, black line) and CW wind phase ($\theta$; red line). Blue, horizontal lines are at $\pm\pi$.

In terms of CW and CCW components this can be rewritten as

$$Covc = \overline{Z_1^- e^{i\omega t}(W_w^- e^{-i\omega t} + W_w^+ e^{i\omega t})} = |Z_1^-||W_w^-|e^{i(\phi-\theta)} \quad (7)$$

and, since $|Z_1^-|$ is virtually equal to $\overline{|Z_1|}$,

$$Cov' = |W_w^-|\cos(\phi - \theta), \quad (8)$$

where $\phi$ and $\theta$ are the respective phases of the CW parts of the current and wind velocity, $W_w^-$ and $W_w^+$ are the CW and CCW rotary components of the wind vector, respectively. The smoothing indicated by the overbar effectively removes contributions from the CCW part of the wind.

$Cov'$ is plotted in Fig. 16(c). It has units of speed and represents the part of the wind speed that is correlated with the current. Where $Cov'$ is positive there is growth in near-inertial energy. This energy diminishes only when $Cov'$ decreases strongly, or becomes negative. Hence, small phase differences ($\phi - \theta$) and large CW wind amplitudes ($|W_w^-|$) correspond to increased $Cov'$ and growing near-inertial energy. The phase ($\phi$) of $|Z_1^-|$ and the phase ($\theta$) of $W_w^-$ is plotted in Fig. 16(d). Both $\phi$ and $\theta$ change slowly with time, with $\theta$ slightly leading. An increasing (decreasing) phase indicates that the actual frequency of the fluctuations is slightly lower (higher) than the 1.0 cpd used in the complex demodulation. The difference between $\theta$ and $\phi$ remains small until about August 31 (Fig. 16(d)) where $\theta$ decreases more rapidly while $\phi$ levels off and then begins to fall after September 2. The differing phase changes result in a loss of coherence between current and wind and after September 2, $Cov'$ falls below zero and $|Z_1^-|$ falls to a local minimum. By September 6, the phases are converging and the near-inertial current amplitudes again increase.

The near-inertial current amplitude and phase relationships for the period between August 18 and September 27, 1997 are shown in Fig. 17. When CW wind and current phases (Fig. 17(c)) are nearly equal (as between day September 7 and 22) the near-inertial amplitude (Fig. 17(a)) grows and is maintained by the CW wind forcing. This provides a clear example of the diurnal wind—near-inertial current resonance. When the wind amplitude decreases (Fig. 17(b)), the near-inertial amplitude levels off and decays (as near September 9). An increase in the CW wind amplitude, when phases are quite different (near September 23), results in

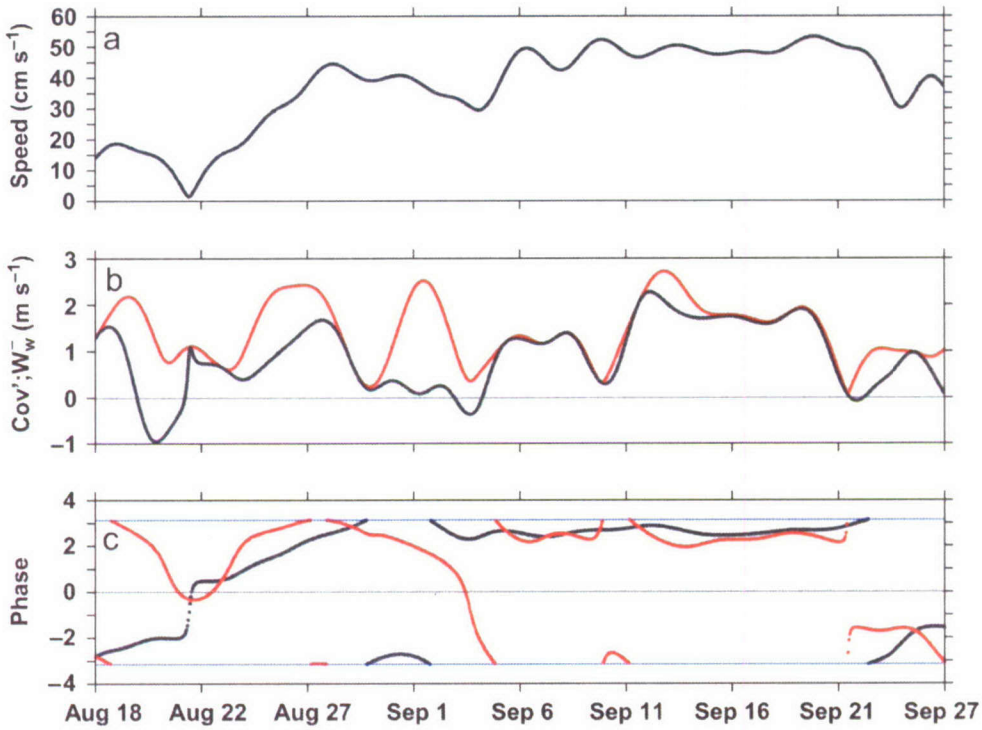


Fig. 17. (a) CW current speed $|Z_1^-|$, for the period shown in Fig. 15. (b) *Cov'* (black line) and $|W_w^-|$ (red line). (c) CW current phase ($\phi$, black line) and CW wind phase ($\theta$; red line). Blue, horizontal lines are at $\pm\pi$.

*Cov'* (Fig. 17(b)) falling and the current amplitude driven downward.

## 8. Summary

Near-inertial currents are common in the northern Gulf of Mexico. Observations collected near the DeSoto Canyon indicate that these currents have amplitudes as large as 40 cm s$^{-1}$. They also show that the near-inertial currents are surface intensified as expected for motions excited by surface forcing (winds). Rotary spectral analysis show distinct CW rotating energy peaks at near-inertial frequencies and little energy in counterclockwise spectra at all analyzed locations

Spatial distributions of CW variance and amplitudes imply that near-inertial energy increased from the shelf break to offshore. This distribution of the near-inertial energy is very different than that observed in the northwestern Gulf where near-inertial currents have a maximum at the shelf break and diminish gradually toward the coast and rapidly offshore (Chen et al., 1996). The lowest near-inertial energy at the shelf break in the DeSoto Canyon region is probably partly related to the fact that the shelf break in this area is near the turning latitude (30°N) for near-diurnal motions. The presence of the largest near-inertial currents over the slope locations could also be related to the trapping of near-inertial energy by negative vorticity generated by energetic mesoscale motion present near the DeSoto Canyon (Hamilton et al., 2000). Enhanced amplitudes of near-inertial currents could also be caused by offshore-propagating near-inertial internal waves and/or trapping of energy by fronts (Tintoré et al., 1995; Davies and Xing, 2005) often present in the DeSoto Canyon region (Hamilton et al., 2000; Jochens et al., 2002).

The variance and CW amplitudes indicate that there is more near-inertial energy in the DeSoto Canyon region during summer months (June–September 1997) than in nonsummer months (November 1997–March 1998). For a given forcing amplitude, an induced near-inertial amplitude will be greater for a shallow mixed layer (D'Asaro, 1985). Due to differences in summer and nonsummer stratifications, the shallower mixed layer is usually present in this region in summer. Thus the difference in the amount of near-inertial energy near the DeSoto Canyon is certainly related to differences in stratification observed in the summer and nonsummer months. A shallower mixed layer

present between June and September 1997 was more inducive to wind forcing and generation of the near-inertial motion.

Near-inertial motions are effectively generated by shifting winds associated with passages of atmospheric fronts, tropical storms, localized thunderstorms, and diurnal atmospheric forcing (sea breeze and daily heating and cooling). In the northwestern Gulf of Mexico, these motions are generally induced by near-diurnal (near-inertial, high-frequency) variations of the wind accompanying passages of cold fronts in winter and spring (Chen et al., 1996). In the DeSoto Canyon region, the largest near-inertial currents are also found to be most effectively excited by high-frequency (near-inertial) wind variations associated with cold front passages between November 1997 and March 1998. For this time period, a simple mixed-layer model forced by the observed wind stress provided a reasonable prediction of the near-inertial currents in the mixed layer.

In summer, however, energetic near-inertial currents in the DeSoto Canyon region often result from resonance between the winds and currents. The resonant excitation of the near-inertial currents by wind forcing near 30°N requires a diurnal wind with a significant CW component with a relatively steady phase that is in phase with any existing near-inertial currents at the onset of the wind. A good example of such an excitation is found in the DeSoto Canyon observations between September 7 and 22, 1997, where the averaged CW near-surface current amplitudes reach $20\,cm\,s^{-1}$ and amplitudes at individual moorings approach $30\,cm\,s^{-1}$, in response to the CW wind amplitudes of about $2\,m\,s^{-1}$. The near-inertial response is quite sensitive to the phase of the periodic forcing, and an increase in the CW forcing amplitude can decrease near-inertial amplitudes if the phases are significantly different.

## Acknowledgments

This work was supported by the Minerals Management Service Environmental Studies Program under Contract 1435-01-04-RP-34601 awarded to Naval Research Laboratory.

## References

Chen, C., Reid, R.O., Nowlin, W.D., 1996. Near-inertial oscillations over the Texas–Louisiana shelf. Journal of Geophysical Research 101 (C2), 3509–3524.

Chereskin, T.K., Morris, M.Y., Niiler, P.P., Kosro, P.M., Smith, R.L., Ramp, S.R., Collins, C.A., Musgrave, D.L., 2000. Spatial and temporal characteristics of the mesoscale circulation of the California Current from eddy-resolving moored and shipboard measurements. Journal of Geophysical Research 105 (C1), 1245–1270.

Crawford, G.B., Large, W.G., 1996. A numerical investigation of resonant inertial response of the ocean to wind forcing. Journal of Physical Oceanography 26, 873–891.

Daddio, E., Wiseman Jr., W.J., Murray, S.P., 1978. Inertial currents over the inner shelf near 30°N. Journal of Physical Oceanography 8, 728–733.

D'Asaro, E.A., 1985. The energy flux from the wind to near-inertial motions in the surface mixed layer. Journal of Physical Oceanography 15, 1043–1059.

D'Asaro, E.A., 1995. Upper-ocean inertial currents forced by a strong storm, part III, interaction of inertial currents and mesoscale eddies. Journal of Physical Oceanography 25, 2953–2958.

Davies, A.M., 1985. Application of a sigma coordinate sea model to the calculation of wind-induced currents. Continental Shelf Research 4, 389–423.

Davies, A.M., Xing, J., 2004. Modelling processes influencing wind-induced internal wave generation and propagation. Continental Shelf Research 24, 2245–2271.

Davies, A.M., Xing, J., 2005. The effect of a bottom shelf front upon the generation and propagation of near-inertial internal waves in the coastal ocean. Journal of Physical Oceanography 35, 976–990.

Denbo, D.W., Allen, J.S., 1984. Rotary empirical orthogonal function analysis of currents near the Oregon coast. Journal of Physical Oceanography 14, 35–46.

DiMarco, S.F., Howard, M.K., Reid, R.O., 2000. Seasonal variation of wind-driven current cycling on the Texas–Louisiana continental shelf. Geophysical Research Letters 27 (7), 1017–1020.

DiMego, G.J., Bosart, L.F., Endersen, G.W., 1976. An examination of the frequency and mean conditions surrounding frontal incursions into the Gulf of Mexico and Caribbean. Monthly Weather Review 104, 709–718.

Federiuk, J., Allen, J.S., 1996. Model studies of near-inertial waves in flow over the Oregon Continental shelf. Journal of Physical Oceanography 26, 2053–2075.

Gutiérrez de Velasco, G., Winant, C.D., 1996. Seasonal patterns of wind stress and wind stress curl over the Gulf of Mexico. Journal Geophysical Research 101 (C8), 18,127–18,140.

Hamilton, P., Berger, T.J., Singer, J.J., Waddell, E., Churchill, J.H., Leben, R.R., Lee, T.N., Sturges, W., 2000. DeSoto Canyon Eddy Intrusion Study, Final Report, Volume II: Technical Report, OSC Study MMS 2000-080. US Department of the Interior, Minerals Management Service, Gulf of Mexico OCS Region, New Orleans, LA, 275pp.

He, R., Weisberg, R.H., 2002. Tides on the West Florida Shelf. Journal of Physical Oceanography 32, 3455–3473.

Henderschott, M.C., 1973. Inertial oscillations of tidal period. Progress in Oceanography 6, 1–27.

Jochens, A.E., DiMarco, S.F., Nowlin Jr., W.D., Reid, R.O., Kennicutt II, M.C., 2002. Northeastern Gulf of Mexico Chemical Oceanography and Hydrography Study: Synthesis Report, OSC Study MMS 2002-055. US Department of the Interior, Minerals Management Service, Gulf of Mexico OCS Region, New Orleans, LA, 586pp.

Krausse, W., 1981. The erosion of the pycnocline. Journal of Physical Oceanography 11, 415–433.

Kundu, P.K., 1976. An analysis of inertial oscillations observed near the Oregon coast. Journal of Physical Oceanography 6, 879–893.

Kunze, E., 1985. Near-inertial wave propagation in geostrophic shear. Journal of Physical Oceanography 15, 544–565.

Large, W.G., Pond, S., 1981. Open ocean momentum flux measurements in moderate and strong winds. Journal of Physical Oceanography 11, 324–336.

Lerczak, J.A., Henderschott, M.C., Winant, C.D., 2001. Observations and modeling of coastal internal waves driven by a diurnal sea breeze. Journal of Geophysical Research 106 (C9), 19,715–19,729.

Millot, C., Crepon, M., 1981. Inertial oscillations on the continental shelf of the Gulf of Lion—observations and theory. Journal of Physical Oceanography 11, 639–657.

Molinari, R.L., Mayer, D.A., 1982. Current meter observations on the continental slope at two sites in the Eastern Gulf of Mexico. Journal of Physical Oceanography 12, 1480–1492.

Morey, S.L., Schroeder, W.W., O'Brien, J.J., Zavala-Hidalgo, J., 2003. The annual cycle of riverine influence in the eastern Gulf of Mexico basin. Geophysical Research Letters 30 (16), 1867.

Orlic, M., 1987. Oscillations at the inertial period on the Adriatic sea shelf. Continental Shelf Research 22, 247–266.

Pawlowicz, R., Beardsley, B., Lentz, S., 2002. Classical tidal harmonic analysis including error estimates in MATLAB using T_TIDE. Computers and Geosciences 28, 929–937.

Perkins, H., 1972. Inertial oscillations in the Mediterranean. Deep-Sea Research 19, 289–296.

Perkins, H., 1976. Observed effect of an eddy on inertial oscillations. Deep-Sea Research 23, 1037–1042.

Pollard, R.T., 1970. On the generation by winds of inertial waves in the ocean. Deep-Sea Research 17, 795–812.

Pollard, R.T., Millard, R.C., 1970. Comparison between observed and simulated wind-generated inertial oscillations. Deep-Sea Research 17, 813–821.

Preisendorfer, R.W., 1988. Principal Component Analysis in Meteorology and Oceanography. Elsevier, Amsterdam, 425pp.

Price, J.F., 1983. Internal wave wake of a moving storm. Part I: scales, energy budget and observations. Journal of Physical Oceanography 13, 949–965.

Shay, L.K., Mariano, A.J., Jacob, S.D., Ryan, E.H., 1998. Mean and near-inertial ocean current response to hurricane Gilbert. Journal of Physical Oceanography 28, 858–889.

Shearman, R.K., 2005. Observations of near-inertial current variability on the New England shelf. Journal of Geophysical Research 110 (C02012).

Simpson, J.H., Hyder, P., Rippeth, T.P., Lucas, I.M., 2002. Forced oscillations near the critical latitude for diurnal-inertial resonance. Journal of Physical Oceanography 32, 177–187.

Tintoré, J., Wang, D.P., Garcia, E., Viúdez, A., 1995. Near-inertial motions in the coastal ocean. Journal of Marine Systems 6, 301–312.

van Haren, H., 2000. Properties of vertical current shear across stratification in the North Sea. Journal of Marine Research 58, 465–491.

Weller, R.A., 1982. The relation of near-inertial motions observed in the mixed layer during the JASIN (1978) experiment to the local wind stress and to the quasi-geostrophic flow field. Journal of Physical Oceanography 12, 1122–1136.

Wiseman Jr., W.J., Rabalais, N.N., Turner, R.E., Dinnel, S.P., MacNaughton, A., 1997. Seasonal and interannual variability within the Louisiana coastal current: stratification and hypoxia. Journal of Marine Systems 12, 237–248.

Xing, J., Davies, A.M., 2003. Influence of coastal effects, bottom topography, stratification, wind period, and mixing upon the propagation of internal waves and the profile of wind-induced currents. Journalof Geophysical Research 108 (C2), 3052.